Evidence for neutron star triaxial free precession in Her X-1 from *Fermi*/GBM pulse period measurements

Dmitry Kolesnikov,[1]★ Nikolai Shakura[1,2] and Konstantin Postnov[1,2]
[1]*Moscow State University, Sternberg Astronomical Institute, 119234 Moscow, Russia*
[2]*Kazan Federal University, 420008 Kazan, Russia*

Accepted XXX. Received YYY; in original form ZZZ

ABSTRACT

Her X-1/HZ Her is one of the best studied accreting X-ray pulsars. In addition to the pulsating and orbital periods, the X-ray and optical light curves of the source exhibit an almost periodic 35-day variability caused by a precessing accretion disk. The nature of the observed long-term stability of the 35-day cycle has been debatable. The pulse period of Her X-1 measured by the *Fermi*/GBM displays periodical variations with X-ray flux at the Main-on state of the source. We explain the observed periodic sub-microsecond pulse frequency changes by a triaxial free precession of the neutron star with parameters previously inferred from an independent analysis of the X-ray pulse evolution over the 35-day cycle.

Key words: X-rays: binaries – X-rays: individual: Her X-1 – stars: neutron

1 INTRODUCTION

Her X-1 is an accreting X-ray pulsar with a pulse period of $P^* = 1.24$ s around the optical star HZ Her with an orbital period of 1.7 days (Tananbaum et al. 1972; Cherepashchuk et al. 1972). The binary system is viewed almost edge-on. This causes different eclipsing features, including periodic orbital eclipses by the optical star and X-ray dips due to gas streams shielding the line of sight (e.g., Shakura et al. 1999). The source also demonstrates a long-term 35-day X-ray flux modulation (Giacconi et al. 1973). It consists of an X-ray bright Main-on state lasting about seven binary orbital periods, followed by a first low state with an almost zero flux (about four orbits), a Short-on state less prominent than the Main-on (about four orbits), and a second low-on state (about four orbits), see Shakura et al. (1998a); Leahy & Wang (2020) for more detail.

The nature of the 35-day modulation has been debatable. One of the first explanation involved a freely precessing neutron star (NS) Brecher (1972); Novikov (1973). For the observed 35-day period to be the NS free precession period $P_{\rm pr}$, an axially symmetric NS should maintain a tiny ellipticity of the order of $\Delta I/I \sim P^*/P_{\rm pr} \sim 10^{-6}$ (here ΔI is the difference in the NS's moments of inertia). In the case of a single NS, the unavoidable internal dissipation would tend to secularly align the spin and precession axes. This argument has been considered disfavoring the NS free precession as the reason for the long-term periodicity in pulsars (e.g., Shaham (1977)). The precession of an accretion disk around NS provides another explanation to the 35-day cycle (e.g., Katz 1973; Roberts 1974; Petterson 1975, and subsequent papers). Presently, a rich phenomenology, both in the X-ray and optical, supports the presence of a tilted, retrograde, precessing accretion disk in Her X-1 (e.g., Boynton et al. 1973; Leahy 2003; Klochkov et al. 2006; Brumback et al. 2021). In the middle of the Main-on and Short-on states, the disk is maximum open to the observer's view, while during the low states, the outer parts of the tilted disk block the X-ray source.

Extensive X-ray observations of Her X-1 demonstrate that there can occur long (with a duration of up to 1.5 years) anomalous low states of the X-ray source during which the X-ray flux is completely extinguished but the X-ray irradiation of the optical star HZ Her persists (Parmar et al. 1985; Vrtilek et al. 1994; Coburn et al. 2000; Boyd et al. 2004; Still & Boyd 2004). These anomalous low states are likely due to vanishing the disk tilt to the orbital plane. As long as the disk tilt is close to zero, the X-ray source remains blocked from the observer's view by the disk's outer parts. An analysis of archive optical observations of HZ Her using photo plates showed that in the past there were periods when the X-ray irradiation effect was absent altogether (Jones et al. 1973; Hudec & Wenzel 1976). This means that sometimes in Her X-1/HZ Her binary system, the accretion onto the neutron star can cease completely (Bisnovatyi-Kogan et al. 1978). The cessation of accretion could occur, for example, because of a sudden jump in the NS magnetic field, which sometimes are observed in Her X-1 (Staubert et al. 2019), or a decrease in the mass inflow from the optical star, which can turn-off accretion due to the propeller effect.

The fact that the 35-day cycle re-appears in phase with the average 35-day ephemeris after the end of anomalous low states and the stable periodic behavior of X-ray pulse profiles Staubert et al. (2013) requires a 'stable clock' mechanism operating in Her X-1/HZ Her (Staubert et al. 2009), which may be the NS free precession. Indeed, a model of two-axial NS free precession can reproduce the observed regular X-ray pulse profile changes with the 35-day phase (Postnov et al. 2013). This model involves a complex non-dipole magnetic field structure near the surface of accreting NS in Her X-1 and pencil-beam local emitting diagram. **The non-dipole surface fields includes additional quadrupole component producing**

★ E-mail: kolesnikovkda@gmail.com

ring-like structures around the NS magnetic poles (Shakura et al. 1991). This additional field doesn't distort the NS's form which is assumed to be shaped by a much stronger internal magnetic field $\sim 10^{14}$ G (Braithwaite 2009). The model also can explain the complicated optical variability of HZ Her over the 35-day cycle, which is primarily shaped by the irradiation effect of the optical star's atmosphere by the X-ray emission from NS (Kolesnikov et al. 2020). A triaxial NS precession in Her X-1 was proposed earlier by us (Shakura et al. 1998b) to explain an anomalously narrow 35-day cycle of Her X-1 observed by HEAO-1. Presently, there is a growing empirical evidence that NS free precession could be responsible for different long-term periodicities in single magnetized NS, such as magnetars and fast radio bursts (FRBs) (see, e.g. Levin et al. 2020; Zanazzi & Lai 2020; Cordes et al. 2021; Wasserman et al. 2021; Makishima et al. 2021).

A precessing, pulsating NS should exhibit regular pulse period (or frequency) variations with a fractional amplitude change of $\Delta P^*/P^* \approx P^*/P_{\rm pr} \sim 10^{-6}$ (e.g, Ruderman 1970; Truemper et al. 1986; Bisnovatyi-Kogan et al. 1989; Bisnovatyj-Kogan & Kahabka 1993; Shakura 1995). This tiny pulse frequency changes of Her X-1 can be searched for by the continuous monitoring of X-ray sources.

In this paper, we show that the periodic sub-microsecond pulse period variability observed in Her X-1 at the 35-day cycle maxima (the Main-on state) by *Fermi*/GBM (Gamma-ray Burst Monitor) (Meegan et al. 2009) can be explained by the motion of X-ray emitting region on the NS surface during the free precession of a triaxial NS. A preliminary analysis of *Fermi*/GBM data for the two-axial NS free precession was reported in Shakura et al. (2021).

2 *FERMI*/GBM X-RAY PULSAR HER X-1 FREQUENCY MEASUREMENTS

Fermi/GBM X-ray pulsar Her X-1 frequency measurements are publicly available[1] and updated on daily basis. The measured frequency $\nu(t)$ of Her X-1 can be represented as a sum of non-periodic long-term frequency variability $\nu_0(t)$ and periodic 35-day frequency variability $\delta\nu(t)$:

$$\nu(t) = \nu_0(t) + \delta\nu(t) \tag{1}$$

or, equivalently, in terms of the angular frequency:

$$\Omega(t) = \Omega_0(t) + \delta\Omega(t)\,. \tag{2}$$

In accreting pulsars like Her X-1, the long-term pulsar frequency trend $\Omega_0(t)$ can be due to changing accretion torques, see Fig. 2.

Assuming that the pulsating flux is emitted near the north magnetic pole N of a rotating solid body, the 35-day periodic variations $\delta\Omega(t)$ are defined by the rate of change of the angle Φ of the spherical triangle $I_3\Omega N$, see Fig. 1:

$$\delta\Omega(t) = \frac{d\Phi(t)}{dt}\,. \tag{3}$$

Here we show that the periodic change of the angle Φ with parameters as in Her X-1 can be explained by a freely precessing NS. We start with considering a two-axial NS precession, which can be treated analytically, and continue with a more general case of triaxial NS free precession.

[1] https://gammaray.nsstc.nasa.gov/gbm/science/pulsars/lightcurves/herx1.html

3 FREE PRECESSION OF THE NEUTRON STAR

3.1 Precession of an axially symmetric NS

It is straightforward to calculate analytically the pulse frequency variations from a freely precessing axially symmetric NS when the NS moments of inertia $I_1 = I_2 \neq I_3$ (see, e.g, Ruderman 1970; Truemper et al. 1986; Bisnovatyi-Kogan et al. 1989; Bisnovatyj-Kogan & Kahabka 1993; Shakura 1995). Below we will assume that the precession frequency is much lower than the spin frequency of the NS so that the total angular momentum vector to a high accuracy coincides with the NS spin vector. When the NS spin frequency vector $\mathbf{\Omega}$ is misaligned with the principal inertia axis I_3 by angle γ, the free precession angular frequency reads

$$\omega = \Omega\,\frac{I_1 - I_3}{I_1}\cos\gamma\,. \tag{4}$$

The observed pulse frequency is modulated by the time derivative of the angle Φ marking the NS precession phase (see Fig. 1). For the angle β between the north magnetic pole N and I_3 axis, the phase Φ can be found from the sine and cosine theorem for spherical triangles:

$$\cos\Phi(t) = \frac{\sin\beta\sin\varphi(t)}{\sqrt{1-[\cos\gamma\cos\beta + \sin\gamma\sin\beta\cos\varphi(t)]^2}}\,, \tag{5}$$

where $\varphi(t)$ is the azimuthal angle of the vector $\mathbf{\Omega}$ in a rigid coordinate frame related to the NS's principal inertia axes (the light grey lines in Fig. 1). In the course of NS free precession, $\varphi(t)$ is a linear function of time:

$$\varphi(t) = \varphi_0 + \omega t\,. \tag{6}$$

The amplitude of the periodic sub-microsecond pulse frequency periodic variations observed by *Fermi*/GBM in Her X-1 can be easily adjusted by assuming a two-axial NS free precession with the appropriate choice of the NS ellipticity $\Delta I/I$ (Shakura et al. 2021). However, the shape of the measured pulse frequency variations as a function of the 35-day phase cannot be adequately reproduced by this model. The situation improves by assuming a slight NS triaxiality, $I_1 \neq I_2 \neq I_3$.

3.2 Precession of a triaxial NS

Given the moments of inertia $I_1 < I_2 < I_3$ and angular velocity $\mathbf{\Omega}$, the NS rotational energy is

$$2E = I_1\Omega_1^2 + I_2\Omega_2^2 + I_3\Omega_3^2, \tag{7}$$

and the angular momentum is

$$M^2 = I_1^2\Omega_1^2 + I_2^2\Omega_2^2 + I_3^2\Omega_3^2. \tag{8}$$

Following Landau & Lifshitz (1976), the motion of the angular momentum vector is described by the equations

$$\Omega_1 = \sqrt{\frac{2EI_3 - M^2}{I_1(I_3 - I_1)}}\,\mathrm{cn}\tau \tag{9}$$

$$\Omega_2 = \sqrt{\frac{2EI_3 - M^2}{I_2(I_3 - I_2)}}\,\mathrm{sn}\tau \tag{10}$$

$$\Omega_3 = \sqrt{\frac{M^2 - 2EI_1}{I_3(I_3 - I_1)}}\,\mathrm{dn}\tau, \tag{11}$$

where $\mathrm{cn}\tau$, $\mathrm{sn}\tau$, $\mathrm{dn}\tau$ are elliptic Jacobi functions, and the dimensionless time τ is

$$\tau = t\sqrt{\frac{(I_3 - I_2)(M^2 - 2EI_1)}{I_1 I_2 I_3}}. \tag{12}$$

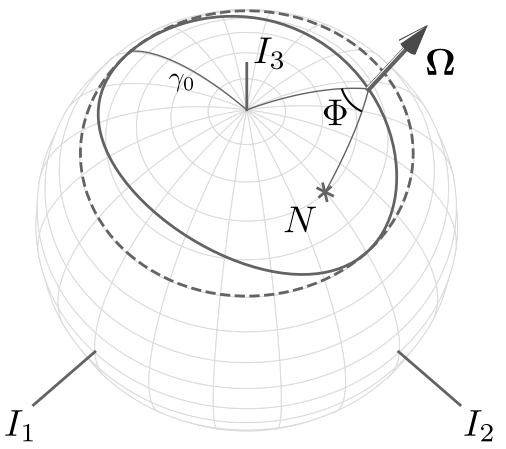

Figure 1. A schematic view of free precession of a triaxial neutron star. The surface coordinates (light grey lines) are related to NS inertial axes I_1, I_2, I_3. The path of the NS angular momentum vector (the spin axis) on the NS surface $\mathbf{\Omega}$ during the triaxial free precession is shown by the solid line. The path of $\mathbf{\Omega}$ during a two-axial free precession is shown by the dashed line. The asterisk marks the north magnetic pole N. Φ is the phase angle of the north magnetic pole N.

The free precession period reads

$$T = 4\sqrt{\frac{I_1 I_2 I_3}{(I_3 - I_2)(M^2 - 2EI_1)}} \int_0^{\pi/2} \frac{du}{\sqrt{1 - k^2 \sin^2 u}}\,, \tag{13}$$

where the parameter k is defined as

$$k^2 = \frac{(I_2 - I_1)(2EI_3 - M^2)}{(I_3 - I_2)(M^2 - 2EI_1)}\,. \tag{14}$$

The fractional moment inertia differences $\Delta I_2 = (I_2 - I_1)/I_1$ and $\Delta I_3 = (I_3 - I_1)/I_1$ are free parameters. The pulsar frequency $\nu = 1/T$ and 35-day cycle periods are defined from observations. Positions of the vector $\mathbf{\Omega}$, phase angle Φ (see Fig. 1) and derivative $d\Phi/dt$ were calculated numerically. We assigned equal values of ΔI_2 for all 35-day cycles to minimize residuals between the model and observations. ΔI_3 was calculated individually for each 35-day cycle to reproduce the actual duration of each 35-day cycle (see Appendix A for the list of 35-day cycle turn-ons determined from the *Swift*/BAT X-ray monitoring of Her X-1).

4 MODELLING OF HER X-1 PULSAR FREQUENCY VARIATIONS

In accreting X-ray pulsars, the long-term pulse frequency variations $\nu_0(t)$ are caused by various factors, e.g. variable accretion torque which are difficult to predict. Here, in order to subtract the long-term pulse frequency variations, we model $\nu_0(t)$ as a cubic spline passing through nodes $\tau_j\,, \nu_0(\tau_j)$ as follows.

We introduce the residuals R between the observed pulsar frequency measurements ν_i at moments t_i and the theoretical model $\nu(t)$:

$$R = \sum_i (\nu(t_i) - \nu_i)^2\,. \tag{15}$$

where the index i runs through all frequency measurements, index j corresponds to the 35-day cycles considered, see Table A1 in Appendix A. Our theoretical model $\nu(t)$ is the sum of the periodic 35-day pulsar frequency variations $d\Phi/dt$ due to the NS free precession and long-term trend $\nu_0(t)$:

$$\nu(t) = \frac{1}{2\pi}\frac{d\Phi(t)}{dt} + \nu_0(t) \tag{16}$$

The time coordinate τ_j of the spline nodes is defined as the mean time of the pulse frequency measurement within the j-th Main-on:

$$\tau_j = \frac{1}{N_j}\sum_i t_i\,, \tag{17}$$

Here, N_j is the number of observations within the j-th Main-on. The spline value $\nu_0(\tau_j)$ is the difference between the mean pulse frequency and the model NS free precession frequency at the moment τ_j:

$$\nu_0(\tau_j) = \frac{1}{N_j}\sum_i \nu_i - \frac{1}{2\pi}\frac{d\Phi(\tau_j)}{dt}\,, \tag{18}$$

The zero free precession phase Φ is assumed to occur be shifted relative to the 35-day cycle beginning t_j by the time interval Δt_j defined as

$$\Delta t_j = \frac{\Delta\varphi}{2\pi} P_j\,. \tag{19}$$

Here $P_j = t_{j+1} - t_j$ is the j-th 35-day cycle duration; the phase lag of the NS free precession zero phase relative to the cycle beginning $\Delta\varphi$ is the model free parameter fixed for all 35-day cycles.

Parameters of the long-term evolution $\nu_0(t)$ and 35-day variations of X-ray pulse frequency $\delta\nu(t)$ were evaluated by minimizing the residuals R, equation 15. Parameters of the triaxial NS free precession are listed in Tables 1 and A1. The minimizing of the residuals R were done using Levenberg–Marquardt algorithm in the LMFIT package (Newville et al. 2014).

The NS free precession $(\Delta I_2, \Delta I_3)$ parameters have been optimized to fit the observed pulse frequency variations measured by *Fermi*/GBM. The NS zero phase shift relative to the 35-day cycle beginning $\Delta\varphi$, ΔI_2 and the NS principal axis of inertia I_3 misalignment with the angular momentum γ_0 were fixed for all 35-day cycles, while ΔI_3 was computed for each cycle to match the $j-th$ cycle duration P_j. The spline nodes values $\{\tau_j, \nu_0(\tau_j)\}$, describing the long-term evolution of the pulsar frequency were also determined from the fitting, see Table B1.

It is worth commenting on the adjustment of the NS free precession period T_j for individual cycles in our global fitting procedure. The trajectory of the NS angular momentum $\mathbf{\Omega}$ on the surface (see Fig. 1) can be defined by $\Delta I_2, \Delta I_3$ and the misalignment angle γ_0 at the NS precession zero phase (cf. Eq. (4) for two-axial case, where this angle is constant). Therefore, the precession period T_j (13) is defined by these three parameters. The 35-day cycle duration P_j in Her X-1 is known to vary by $\lesssim \pm 5\%$ (see Table A1 in the Appendix for our data analysis). Assuming the NS free precession as the 35-day clock, the precession period variations can be accounted for by changing one of these parameters (for example, the relative inertia moment difference ΔI_3 with constant ΔI_2 and γ_0, or the angle γ_0 with constant I_1, I_2, I_3). Moment of inertia variations correspond to not a fully rigid body; the variations of misalignment between the NS principal inertia axis I_3 and angular momentum can be due to internal coupling between the NS crust and core. Both cases are physically plausible for a realistic NS. In Table A1 (the last columns) we provide ΔI_3 for individual 35-day cycles (assuming constant ΔI_2 and γ_0). In Fig. 5, we plot the free precession period

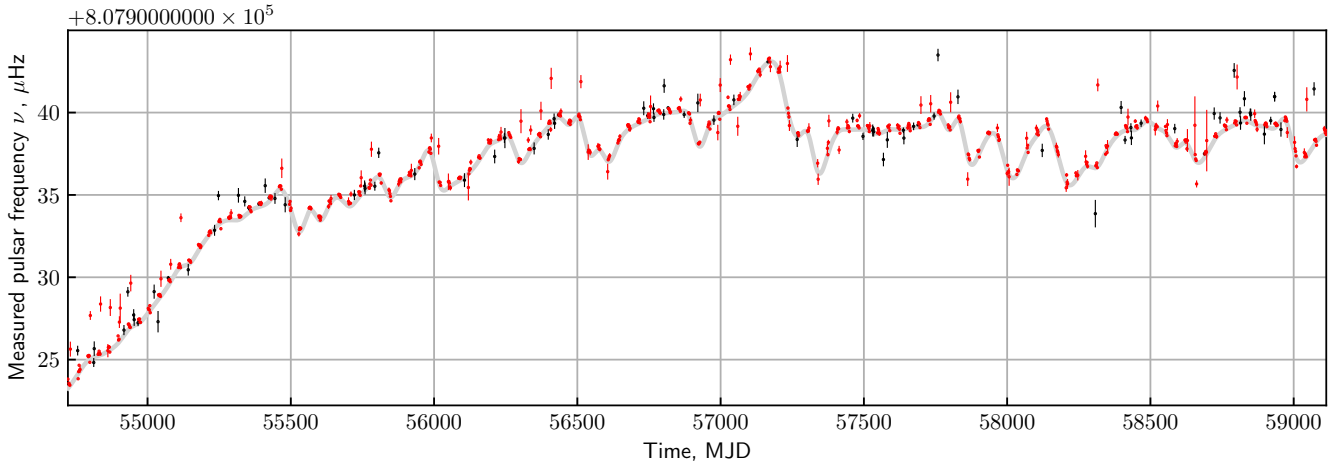

Figure 2. Her X-1 pulse frequency as a function of time. The dots show *Fermi*/GBM measurements (in red during the 35-day cycle Main-on phases 0.0–0.35, in black otherwise). The grey solid line shows the long-term pulse frequency variations $\nu_0(t)$ approximated as described in Section 4.

Table 1. Triaxial free precession model parameters fixed during the global fitting

Parameter	Symbol	Value
Ω and I_3 axis misalignment at zero free precession phase	γ_0	50°
Coordinates of the magnetic pole N	N_ϕ N_θ	90° 30°
Relative inertia moment difference $(I_2 - I_1)/I_1$	ΔI_2	3×10^{-7}
Phase shift of free precession zero phase relative to the 35-day cycle beginning	$\Delta\varphi$	−0.096

T (13) for fiducial values $\Delta I_2 = 3 \times 10^{-7}$ and $\Delta I_3 = 6.37 \times 10^{-7}$ corresponding to $T \approx 35$ days, as a function of the angle γ_0. In both cases, a few % variations in the parameters alter the free precession period T correspondingly. Therefore, our NS free precession model for Her X-1 suggests a few % change in the NS body parameters from cycle to cycle. Similar indications have been obtained earlier from the analysis of O-C behaviour of the mean 35-day cycle duration (Postnov et al. 2013).

The best-fit modeling of the periodic X-ray pulse variations of Her X-1 by the triaxial NS free precession with parameters from Table 1 is shown in Figs. 3 and 4. The solid black line presents the model $\nu(t)$, with the duration of each 35-day cycle adjusted using the fractional moment inertial difference ΔI_3 listed in Table A1. The vertical lines marks the 35-day line starts t_j from Table A1. The NS free precession zero phases correspond to the local minima between two maxima preceding the 35-day cycle turn-ons by the constant phase $|\Delta\phi| = 0.096$. Therefore, in this model, the observed pulse frequency modulation is produced by the 'descending' branch of the $\nu(t)$. The symmetric 'ascending' branch of $\nu(t)$ before the NS zero phase falls on the Short-on state of Her X-1 where pulse frequency measurements have large errors. The future more precise X-ray timing observations are required to test the predict behaviour $\nu(t)$ and to improve upon the model parameters.

5 DISCUSSION & CONCLUSION

The 0.3–0.5 microsecond variability of the X-ray pulse period of Her X-1 measured by *Fermi*/GBM[2] with ∼ 0.1 microsec accuracy suggests the emitting region radial velocity amplitude $V_r/c \leq \Delta P^*/P^* = \Delta\nu^*/\nu^* \sim 3 \times 10^{-7}$. In principle, besides the NS free precession, such a variability could be generated by reflection from the warped accretion disk precessiong with the angular velocity ω_{pr}. In that case, the maximum radial velocity of the reflector should be $V_{r,max} = \omega_{pr} R_{in} \approx 2 \times 10^2$ cm/s for the assumed inner disk radius $R_{in} \approx 10^8$ cm. This velocity would give rise to the Doppler frequency modulation with an amplitude of $\Delta\nu_{ref}/\nu^* \sim 10^{-8}$, much smaller than the observed value. The Doppler broadening of the reprocessed pulsations on the accretion disk flow would smear the precession-induced frequency variations. Therefore, the possibility that the observed pulsar period change is due to reprocession of the X-ray pulses on the disk seems unlikely.

In our model, the inner part of the disk should align with the NS's equator due to magnetic forces (Lipunov & Shakura 1980; Lipunov et al. 1981; Lai 1999) during the 35-day cycle Main-on. The pulsar period 1.24 s should be close to the equilibrium value (the magnetospheric radius is close to the corotation radius), suggesting the inner disk radius ∼ 100 R_{ns}. Therefore, the accreting plasma gets frozen into the magnetic field and is canalised onto the NS's surface in regions defined by the local magnetic field structure. In this case, the precession of the outer parts of the disk does not produce variations of the hot spot geometry.

During the Short-on stage, the X-ray flux is several times as low as at the Main-on, and the pulse period determination from *Fermi*/GBM data is less certain. However, on several occasions (e.g., on MJD 54952, 55757, 56418, 57532) the pulse period is found to be at the approximately the same level as at the Main-on[2]. In our model, the Short-on pulse is shaped by emitting arcs located symmetrically to the inertia axis I_3 but phase-separated by π (see Fig. 2 and 3 in Postnov et al. 2013). Therefore, the expected pattern of the pulse profile variations during the Short-on should be similar to the Main-

[2] https://gammaray.nsstc.nasa.gov/gbm/science/pulsars/lightcurves/herx1.html

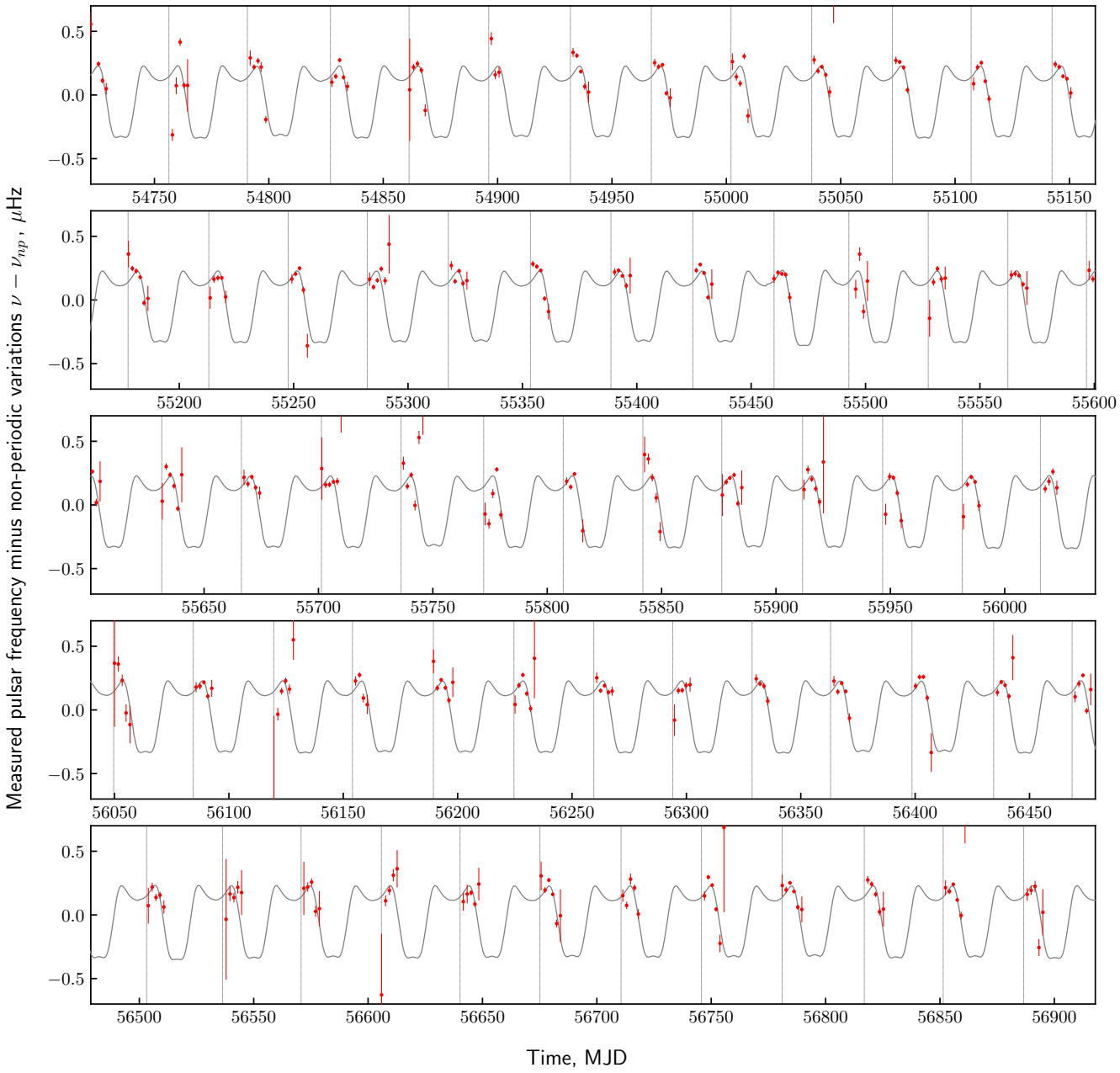

Figure 3. Her X-1 pulsar frequency minus non-periodic variations $\nu - \nu_0$ as a function of time. Time coverage MJD 54725–56919 (for MJD 56919–59113, see Fig. 4). Red dots show the *Fermi*/GBM measurements. Only points at phases 0.05–0.20 of 35-day cycle are shown. The gray solid line indicates model periodic variation of the pulsar frequency due to NS free precession. The model calculated as described in Section 3.2. The irregular non-periodic variations ν_0 calculated as described in Section 4. The vertical lines shows the turn-on times of 35-day cycles, calculated as described in Section A.

on. Future accurate measurements of the X-ray pulse timing in Her X-1 could be used to test this prediction.

We conclude that a freely precessing NS in Her X-1 with parameters inferred from an independent analysis of X-ray pulse profile evolution with 35-day phase (Postnov et al. 2013) can explain regular sub-microsecond pulse period changes observed by *Fermi*/GBM. **To explain a few % variations in the individual 35-cycle duration, the model requires the corresponding change in the NS parameters (relative difference in the moments of inertia or the NS angular momentum misalignment with the principal moment of inertia). These changes might be related to the variable internal coupling of the NS crust with the core.** The model has also proved successful in explaining the HZ Her optical light curves over the 35-day cycle as well (Kolesnikov et al. 2020). Therefore, after about half century of studies, the NS free precession as the inner clock mechanism for the observed 35-day cycle in Her X-1/HZ Her is further supported by the pulse period

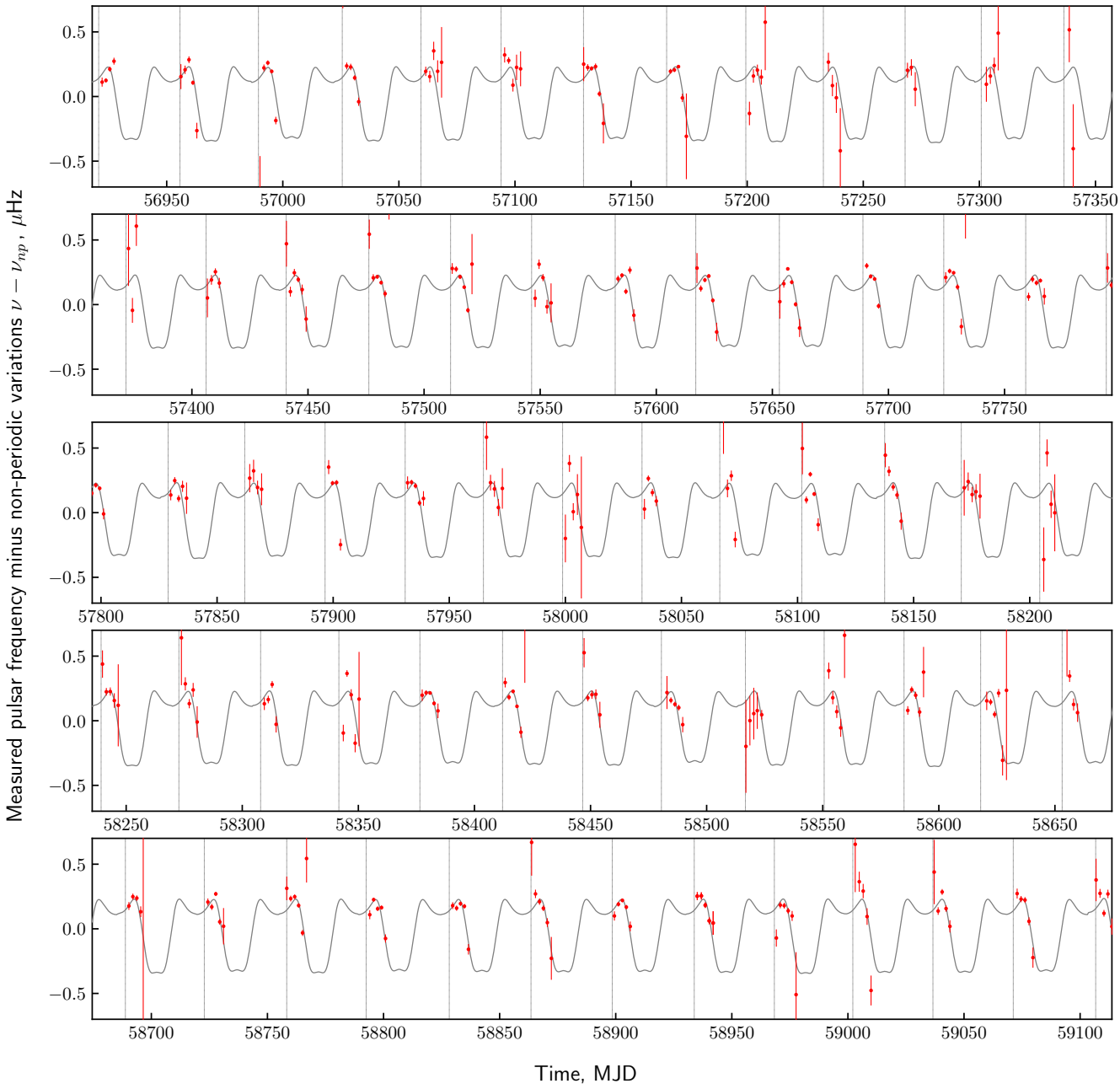

Figure 4. The same as the Fig. 3, time coverage MJD 56919–59113.

ACKNOWLEDGEMENTS

The work of DK and NS was supported by the RSF grant 21-12-00141 (modelling of Her X-1 pulsar frequency variations; calculation of *Swift*/BAT 35-day cycle turn-on times). The authors are supported by the Interdisciplinary Scientific Educational School of Moscow University 'Fundamental and applied space research' (two- and triaxial NS free precession analytical model analysis).

DATA AVAILABILITY

The data underlying this article are available in the article, *Fermi*/GBM X-ray data are freely available at https://gammaray.nsstc.nasa.gov/gbm/science/pulsars/lightcurves/herx1.html, *Swift*/BAT X-ray data are freely available at https://swift.gsfc.nasa.gov/results/transients/HerX-1/.

REFERENCES

Alexander T., 1997, Is AGN Variability Correlated with Other AGN Proper-

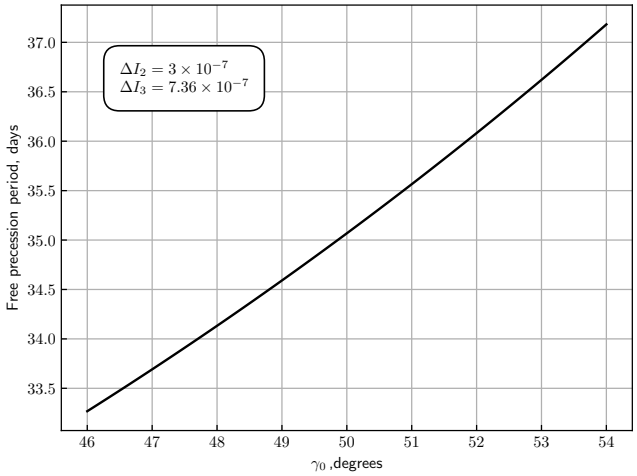

Figure 5. Caption

ties? ZDCF Analysis of Small Samples of Sparse Light Curves. Springer, p. 163, doi:10.1007/978-94-015-8941-3_14
Bisnovatyi-Kogan G. S., Bochkarev N. G., Karitskaia E. A., Cherepashchuk A. M., Shakura N. I., 1978, Soviet Astronomy Letters, 4, 43
Bisnovatyi-Kogan G. S., Mersov G. A., Shefer E. K., 1989, A&A, 221, L7
Bisnovatyj-Kogan G. S., Kahabka P., 1993, A&A, 267, L43
Boyd P., Still M., Corbet R., 2004, The Astronomer's Telegram, 307, 1
Boynton P. E., Canterna R., Crosa L., Deeter J., Gerend D., 1973, ApJ, 186, 617
Braithwaite J., 2009, MNRAS, 397, 763
Brecher K., 1972, Nature, 239, 325
Brumback M. C., Hickox R. C., Fürst F. S., Pottschmidt K., Tomsick J. A., Wilms J., Staubert R., Vrtilek S., 2021, ApJ, 909, 186
Cherepashchuk A. M., Efremov Y. N., Kurochkin N. E., Shakura N. I., Sunyaev R. A., 1972, Information Bulletin on Variable Stars, 720
Coburn W., et al., 2000, ApJ, 543, 351
Cordes J. M., Wasserman I., Chatterjee S., Batra G., 2021, arXiv e-prints, p. arXiv:2107.12874
Giacconi R., Gursky H., Kellogg E., Levinson R., Schreier E., Tananbaum H., 1973, ApJ, 184, 227
Hudec R., Wenzel W., 1976, Bulletin of the Astronomical Institutes of Czechoslovakia, 27, 325
Jones C. A., Forman W., Liller W., 1973, ApJ, 182, L109
Katz J. I., 1973, Nature Physical Science, 246, 87
Klochkov D. K., Shakura N. I., Postnov K. A., Staubert R., Wilms J., Ketsaris N. A., 2006, Astronomy Letters, 32, 804
Kolesnikov D. A., et al., 2020, MNRAS, 499, 1747
Lai D., 1999, ApJ, 524, 1030
Landau L. D., Lifshitz E. M., 1976, in Landau L., Lifshitz E., eds, , Mechanics (Third Edition), third edition edn, Butterworth-Heinemann, Oxford, pp 96–130, doi:https://doi.org/10.1016/B978-0-08-050347-9.50011-3
Leahy D. A., 2003, MNRAS, 342, 446
Leahy D., Wang Y., 2020, ApJ, 902, 146
Levin Y., Beloborodov A. M., Bransgrove A., 2020, ApJ, 895, L30
Lipunov V. M., Shakura N. I., 1980, Soviet Astronomy Letters, 6, 14
Lipunov V. M., Semenov E. S., Shakura N. I., 1981, Azh, 58, 765
Makishima K., Tamba T., Aizawa Y., Odaka H., Yoneda H., Enoto T., Suzuki H., 2021, arXiv e-prints, p. arXiv:2109.11150
Meegan C., et al., 2009, ApJ, 702, 791
Newville M., Stensitzki T., Allen D. B., Ingargiola A., 2014, LMFIT: Non-Linear Least-Square Minimization and Curve-Fitting for Python, doi:10.5281/zenodo.11813, https://doi.org/10.5281/zenodo.11813
Novikov I. D., 1973, Soviet Ast., 17, 295
Parmar A. N., Pietsch W., McKechnie S., White N. E., Truemper J., Voges W., Barr P., 1985, Nature, 313, 119
Petterson J. A., 1975, ApJ, 201, L61
Postnov K., Shakura N., Staubert R., Kochetkova A., Klochkov D., Wilms J., 2013, MNRAS, 435, 1147
Roberts W. J., 1974, ApJ, 187, 575
Ruderman M., 1970, Nature, 225, 838
Shaham J., 1977, ApJ, 214, 251
Shakura N. I., 1995, HER X-1/HZ Her: 35-day Cycle, Freely Precessing Neutron Star and Accompanying Effects. Nova Science Publishers, p. 55
Shakura N. I., Postnov K. A., Prokhorov M. E., 1991, Soviet Astronomy Letters, 17, 339
Shakura N. I., Ketsaris N. A., Prokhorov M. E., Postnov K. A., 1998a, MNRAS, 300, 992
Shakura N. I., Postnov K. A., Prokhorov M. E., 1998b, A&A, 331, L37
Shakura N. I., Prokhorov M. E., Postnov K. A., Ketsaris N. A., 1999, A&A, 348, 917
Shakura N. I., Kolesnikov D. A., Postnov K. A., 2021, arXiv e-prints, p. arXiv:2103.01820
Staubert R., Bezler M., Kendziorra E., 1983, A&A, 117, 215
Staubert R., Klochkov D., Postnov K., Shakura N., Wilms J., Rothschild R. E., 2009, A&A, 494, 1025
Staubert R., Klochkov D., Vasco D., Postnov K., Shakura N., Wilms J., Rothschild R. E., 2013, A&A, 550, A110
Staubert R., et al., 2019, A&A, 622, A61
Still M., Boyd P., 2004, ApJ, 606, L135
Tananbaum H., Gursky H., Kellogg E. M., Levinson R., Schreier E., Giacconi R., 1972, ApJ, 174, L143
Truemper J., Kahabka P., Oegelman H., Pietsch W., Voges W., 1986, ApJ, 300, L63
Vrtilek S. D., et al., 1994, ApJ, 436, L9
Wasserman I., Cordes J. M., Chatterjee S., Batra G., 2021, arXiv e-prints, p. arXiv:2107.12911
Zanazzi J. J., Lai D., 2020, ApJ, 892, L15

APPENDIX A: *SWIFT*/BAT 35-DAY CYCLE TURN-ON TIMES

Usually, in order to determine the duration of 35-day cycles of Her X-1, the cross-correlation function (CCF) of X-ray flux data with a 35-day flux template is calculated (see, e.g. Klochkov et al. 2006; Leahy & Wang 2020). The CCF maxima correspond to the best fit of the template and measured data.

We analyzed *Swift*/BAT X-ray monitoring of Her X-1. As a template, the X-ray flux data between MJD 55700–55736 covering one 35-day cycle of Her X-1 were used. The choice of this particular cycle was arbitrary; other cycles are also applicable except those with a small number of observations or long gaps. We excluded data in the orbital phase interval ±0.16 near the eclipse center to minimize the X-ray flux orbital modulation.

To calculate CCF, a z-transformed discrete correlation algorithm (ZDCF) was applied (Alexander 1997). The algorithm produces CCF which takes maximum values at time moments $t_j^{\rm CCF}$ corresponding to the best matching of the template with data. False CCF maxima, which arise when the template Main-on coincides with the data Short-ons, were deleted manually. The phase $\varphi_i^{\rm CCF}$ of the individual flux measurement at time t_i inside the j-th cycle $t_j \le t_i < t_{j+1}$ reads:

$$\varphi_i^{\rm CCF} = \frac{t_i - t_j^{\rm CCF}}{t_{j+1}^{\rm CCF} - t_j^{\rm CCF}} \,. \qquad \text{(A1)}$$

All data points phased in this were binned in 350 intervals. The average X-ray flux in the bin $\langle F \rangle$ and its standard deviation σ were calculated in each bin. The beginning of the 35-day cycle is defined as the first bin with $\langle F \rangle / \sigma > 3$. The coordinate of the bin is the

phase $\varphi_b^{\rm CCF}$ of the 35-day cycle beginning. To find the moment t_j of the 35-day cycle beginning, the time difference $\varphi_b^{\rm CCF} P_j$ should be added to the corresponding moment $t_j^{\rm CCF}$ of the CCF maximum:

$$t_j = t_j^{\rm CCF} + \varphi_b^{\rm CCF} P_j \,, \tag{A2}$$

where $P_j = t_{j+1}^{\rm CCF} - t_j^{\rm CCF}$ is duration of the j-th cycle. In Table A1, the obtained turn-on moments t_j are presented. The numbering of 35-day cycles follows the convention introduced by Staubert et al. (1983). The accuracy of the method is limited by the bin width. The use of 350 bins over 35 days results in an 0.1-day uncertainty in t_j, sufficient to model Her X-1 pulsar frequency variations.

APPENDIX B: HER X-1 LONG-TERM PULSE FREQUENCY EVOLUTION

Here we present table of the spline values τ_j , $\nu_0(\tau_j)$ of the long-term evolution of Her X-1 pulse frequency. The method of calculation of τ_j , $\nu_0(\tau_j)$ is described in Section 4.

Table A1. 35-day cycles

Cycle number j	Cycle start t_j MJD	Cycle duration P_j days	ΔI_3 $\times 10^{-7}$
382	54650.9	34.7	6.422
383	54685.6	34.0	6.549
384	54719.6	35.3	6.306
385	54755.0	34.1	6.543
386	54789.1	35.6	6.257
387	54824.7	34.3	6.503
388	54858.9	35.6	6.262
389	54894.5	35.4	6.304
390	54929.9	35.6	6.26
391	54965.5	34.6	6.437
392	55000.1	35.6	6.253
393	55035.8	35.6	6.259
394	55071.4	34.3	6.503
395	55105.6	35.5	6.282
396	55141.1	35.3	6.305
397	55176.5	35.4	6.296
398	55211.9	33.9	6.581
399	55245.7	35.7	6.247
400	55281.4	34.6	6.437
401	55316.0	35.2	6.325
402	55351.3	36.0	6.19
403	55387.3	35.1	6.341
404	55422.4	34.9	6.383
405	55457.3	33.3	6.688
406	55490.6	35.4	6.294
407	55526.0	34.7	6.418
408	55560.8	34.3	6.492
409	55595.1	35.2	6.322
410	55630.4	34.5	6.456
411	55664.9	35.2	6.325
412	55700.1	34.9	6.377
413	55735.1	35.9	6.206
414	55771.0	34.7	6.422
415	55805.7	34.1	6.535
416	55839.8	34.9	6.381
417	55874.7	36.0	6.197
418	55910.7	34.6	6.435
419	55945.3	34.2	6.522
420	55979.5	35.0	6.376
421	56014.4	34.2	6.513
422	56048.6	34.9	6.378
423	56083.6	34.6	6.44
424	56118.2	34.4	6.485
425	56152.6	35.3	6.313
426	56187.9	34.6	6.438
427	56222.5	35.8	6.232
428	56258.2	34.7	6.426
429	56292.9	34.4	6.484
430	56327.3	34.6	6.437
431	56361.9	35.1	6.343
432	56397.0	35.2	6.33
433	56432.3	34.4	6.47
434	56466.7	35.6	6.269
435	56502.3	33.0	6.748

Table A1 – *continued* 35-day cycles

Cycle number j	Cycle start t_j MJD	Cycle duration P_j days	ΔI_3 $\times 10^{-7}$
436	56535.3	34.1	6.53
437	56569.4	34.0	6.546
438	56603.5	35.9	6.2
439	56639.4	33.7	6.605
440	56673.1	35.5	6.271
441	56708.7	35.7	6.25
442	56744.3	35.8	6.221
443	56780.2	35.3	6.314
443	56815.5	35.0	6.362
445	56850.5	33.5	6.661
446	56884.0	35.6	6.262
447	56919.5	33.7	6.622
448	56953.2	34.6	6.444
449	56987.8	36.2	6.156
450	57024.0	34.6	6.447
451	57058.6	34.2	6.525
452	57092.7	35.5	6.281
453	57128.2	35.3	6.321
454	57163.5	34.5	6.459
455	57198.0	32.8	6.794
456	57230.8	33.7	6.616
457	57264.4	35.0	6.371
458	57299.4	33.6	6.624
459	57333.1	35.9	6.21
460	57369.0	35.0	6.362
461	57404.0	35.8	6.233
462	57439.7	35.2	6.34
463	57474.9	34.7	6.415
464	57509.6	35.1	6.341
465	57544.8	36.2	6.158
466	57581.0	34.4	6.48
467	57615.4	36.8	6.06
468	57652.2	35.5	6.286
469	57687.6	35.1	6.341
470	57722.8	35.2	6.333
471	57758.0	34.7	6.414
472	57792.7	33.0	6.744
473	57825.7	32.8	6.796
474	57858.5	36.4	6.127
475	57894.9	33.9	6.573
476	57928.8	35.5	6.274
477	57964.3	32.6	6.844
478	57996.9	34.7	6.421
479	58031.6	33.7	6.623
480	58065.3	35.7	6.246
481	58100.9	34.1	6.532
482	58135.1	34.1	5.539
483	58169.1	32.8	6.796
484	58201.9	33.9	6.572
485	58235.9	36.8	6.059
486	58272.6	33.8	6.59
487	58306.4	35.1	6.357
488	58341.5	32.4	6.887
489	58373.9	36.4	6.116
490	58410.3	35.6	6.254
491	58445.9	34.4	6.47
492	58480.4	35.9	6.2
493	58516.3	33.4	6.675
494	58549.7	32.3	6.891
495	58582.1	35.0	6.374
496	58617.0	35.1	6.351
497	58652.1	34.6	6.442

Table A1 – *continued* 35-day cycles

Cycle number j	Cycle start t_j MJD	Cycle duration P_j days	ΔI_3 $\times 10^{-7}$
498	58686.7	34.1	6.527
499	58720.9	35.7	6.242
500	58756.6	35.1	6.348
501	58791.7	35.5	6.279
502	58827.2	35.3	6.318
503	58862.4	34.4	6.478
504	58896.9	36.6	6.097
505	58933.4	33.5	6.653
505	58966.9	33.7	6.61
507	59000.6	35.2	6.332
508	59035.8	35.1	6.344
509	59070.9	34.3	6.493
510	59105.3	33.0	6.754
511	59138.3	35.6	6.254
512	59173.9	34.3	6.49
513	59208.2	35.1	6.358
514	59243.3	35.1	6.351
515	59278.4	34.1	6.53
516	59312.5	35.6	6.257
517	59348.1	34.8	6.4
518	59382.9	34.7	6.42

Table B1. Pulse frequency long-term evolution

Cycle number j	τ_j MJD	$\nu_0(\tau_j) \times 10^{-5} + 0.8079$, Hz
383	54726.91	2.3476
385	54760.36	2.4355
386	54796.05	2.5070
387	54831.80	2.5380
388	54865.80	2.5659
389	54900.66	2.6082
390	54936.37	2.6978
391	54971.21	2.7340
392	55006.07	2.8031
393	55041.76	2.8834
394	55076.63	2.9694
395	55112.33	3.0662
396	55146.33	3.0910
397	55182.04	3.1806
398	55216.88	3.2679
399	55251.74	3.3362
400	55287.45	3.3517
401	55321.46	3.3598
402	55357.15	3.4129
403	55392.85	3.4379
404	55428.56	3.4796
405	55464.27	3.5462
406	55498.27	3.4341
407	55531.43	3.2819
408	55567.13	3.4153
409	55601.13	3.3524
410	55635.97	3.4482

Table B1 – *continued* Pulse frequency long-term evolution

Cycle number j	τ_j MJD	$\nu_0(\tau_j) \times 10^{-5} + 0.8079$, Hz
411	55670.85	3.4878
412	55705.68	3.4367
413	55741.39	3.4997
414	55777.10	3.5698
415	55810.62	3.6085
416	55845.94	3.4974
417	55880.79	3.5782
418	55916.50	3.6168
419	55951.36	3.6936
420	55986.21	3.7729
421	56019.37	3.5627
422	56053.36	3.5510
422	56089.08	3.5909
424	56123.93	3.6445
425	56157.93	3.7143
426	56193.66	3.8105
427	56229.34	3.8463
428	56264.19	3.8520
429	56299.04	3.7043
430	56333.04	3.7663
431	56368.75	3.8619
432	56403.61	3.9323
433	56438.46	3.9829
434	56473.31	3.9383
435	56508.17	3.9673
436	56541.32	3.7576
437	56575.32	3.7831
438	56609.32	3.7088
439	56645.02	3.8269
440	56679.87	3.9120
441	56714.75	3.9438
442	56750.44	3.9712
443	56785.31	3.9958
444	56821.00	4.0038
445	56856.69	4.0148
446	56891.56	3.9804
447	56924.70	3.7997
448	56959.57	3.9324
449	56994.40	3.9863
450	57030.10	4.0276
451	57064.13	4.0673
452	57099.84	4.1381
453	57133.83	4.2445
454	57169.52	4.3165
455	57204.38	4.2516
456	57236.69	3.9947
457	57269.85	3.8602
458	57305.56	3.8793
459	57339.56	3.6466
460	57375.24	3.7617
461	57410.11	3.8909
462	57444.96	3.9009
463	57480.66	3.9054
464	57516.37	3.9028
465	57551.23	3.8788
466	57586.08	3.9012
467	57621.77	3.9046
468	57657.47	3.9111
469	57693.46	3.9164
470	57728.89	3.9432
471	57762.88	3.9992
472	57798.58	3.9025
473	57832.60	3.9695

Table B1 – *continued* Pulse frequency long-term evolution

Cycle number j	τ_j MJD	$\nu_0(\tau_j) \times 10^{-5} + 0.8079$, Hz
474	57865.75	3.7353
475	57900.60	3.7525
476	57935.46	3.8704
477	57969.45	3.8382
478	58003.45	3.6421
479	58036.61	3.6337
480	58070.63	3.7774
481	58105.48	3.8695
482	58141.17	3.9264
483	58175.18	3.7653
484	58208.36	3.5862
485	58243.18	3.6102
486	58277.18	3.6743
487	58312.04	3.6719
488	58346.89	3.7699
489	58380.89	3.8702
490	58416.61	3.9037
491	58450.59	3.8997
492	58486.31	3.9490
493	58521.13	3.9164
494	58556.02	3.8763
495	58589.17	3.8031
496	58624.88	3.8219
497	58658.09	3.7112
498	58692.78	3.7505
499	58726.88	3.8553
500	58762.58	3.9048
501	58797.45	3.9344
502	58832.30	3.9583
503	58868.00	3.9290
504	58902.00	3.9213
505	58937.69	3.9152
506	58973.42	3.9562
507	59006.56	3.7438
508	59041.41	3.7264
509	59075.41	3.8179
510	59110.27	3.8715
511	59144.27	3.9584
512	59179.14	4.0506
513	59213.98	4.0771
514	59248.84	4.1086
515	59283.68	4.1487
516	59318.54	4.2293
517	59352.54	4.2662
518	59389.16	4.3000